



# Lens Distortion Measurement and Correction for Stereovision Multi-Camera System <sup>†</sup>

Grzegorz Madejski <sup>1,\*</sup>, Sebastian Zbytniewski <sup>1</sup>, Mateusz Kurowski <sup>1</sup>, Dawid Gradolewski <sup>1</sup>, Włodzimierz Kaoka <sup>1</sup> and Wlodek J. Kulesza <sup>2</sup>

<sup>1</sup> Bioseco S. A., Budowlanych 68, 80-298 Gdansk, Poland; sebastian.zbytniewski@bioseco.com (S.Z.); mateusz.kurowski@bioseco.com (M.K.); dawid.gradolewski@bioseco.com (D.G.); wlodzimierz.kaoka@bioseco.com (W.K.)

<sup>2</sup> Department of Mathematics and Natural Sciences, Blekinge Institute of Technology, 371 79 Karlskrona, Sweden; wlodek.kulesza@bth.se

\* Correspondence: grzegorz.madejski@bioseco.com

<sup>†</sup> Presented at the 11th International Electronic Conference on Sensors and Applications (ECSA-11), 26–28 November 2024; Available online: <https://sciforum.net/event/ecsa-11>.

**Abstract:** In modern autonomous systems, measurement repeatability and precision are crucial for robust decision-making algorithms. Stereovision, which is widely used in safety applications, provides information about the object's shape, orientation, and 3D-localisation. The camera's lens distortion is a common source of systematic measurement errors, which can be estimated and then eliminated or at least reduced using a suitable correction/calibration method. In this study, a set of cameras equipped with Basler Lenses (C125-0618-5M F1.8 f6mm) and Sony IMX477R matrices are calibrated using a state-of-the-art Zhang-Duda-Frese method. The resulting distortion coefficients are used to correct the images. The calibrations are evaluated with the aid of two novel methods of lens distortion measurement. The first one is based on linear regression with images of a vertical and horizontal line pattern. Based on the evaluation tests, outlying cameras are eliminated from the test set by applying the  $2\sigma$  criterion. For the remaining cameras, the MSE was reduced up to 75.4 times, to 1.8 px–6.9 px. The second method is designed to evaluate the impact of lens distortion on stereovision applied to bird tracking around wind farms. The bird's flight trajectory is synthetically generated to estimate changes in disparity and distance before and after calibration. The method shows that, on the margins of the image, lens distortion might introduce errors in the object's distance measurement of +17%–+20% for cameras with the same distortion and from –41% up to  $+\infty$  for camera pairs with different lens distortion. The results highlight the importance of having well-calibrated cameras in systems that require precision, such as stereovision bird tracking for bird-turbine collision risk assessment systems.

**Keywords:** evaluation methods; image processing; image transformation; intrinsic parameters; lenses; linear regression; optical sensors; stereo-vision



**Citation:** Madejski, G.; Zbytniewski, S.; Kurowski, M.; Gradolewski, D.; Kaoka, W.; Kulesza, W.J. Lens Distortion Measurement and Correction for Stereovision Multi-Camera System. *Eng. Proc.* **2024**, *1*, 0. <https://doi.org/>

Academic Editor: Firstname  
Lastname  
Published: 26 November 2024



**Copyright:** © 2024 by the authors. Licensee MDPI, Basel, Switzerland. This article is an open access article distributed under the terms and conditions of the Creative Commons Attribution (CC BY) license (<https://creativecommons.org/licenses/by/4.0/>).

## 1. Introduction

Reliable infrastructure monitoring has become a cornerstone of Industry 5.0 allowing autonomisation of modern industry with the use of state-of-the-art technologies [1]. There are many technologies, such as vision sensors, radar, and lidar enabling collaboration of humans and systems [2]. Their use depends on many factors, e.g., distance, size of the observed object, required robustness or accuracy. For vision-based systems, the quality of images plays a crucial role. There are many factors that affect the image quality. One of the vital problems can be lens distortion, which reduces the precision of vision and distorts the viewed object's size, shape, and localisation at the image plane. Despite being manufactured within a range of identical specifications, the lens distortion coefficients and

other intrinsic parameters of cameras often exhibit slight variations due to factors like component manufacturing inconsistencies, differences in the assembly process, environmental conditions, and prolonged use.

Therefore, for image-based monitoring systems, ensuring the precise calibration of cameras is essential for maintaining performance quality. This research focuses on the calibration of the Bird Protection System (BPS) by Bioseco [3,4], an advanced technology designed to prevent bird collisions with wind turbines and other large structures. BPS relies on multi-stereoscopic cameras to detect and track birds in real-time. In this study, we address the problem of distortion calibration that can improve stereo-vision-based distance measurement. The problem of distortion variation among cameras and the possibility of using a correction method that could ensure correction consistency is analysed. We show that the calibration can significantly improve the accuracy of distance measurement. Nevertheless, we conclude that to achieve the required accuracy, each camera must be corrected separately.

## 2. Background Knowledge and Review of Related Works

In computer vision, a projection of a 3D point  $\mathbf{P}_{world}$  in the world onto the 2D image plane as a point  $\mathbf{P}_{img}$  for a pin-hole camera model is described by the following formula:

$$\mathbf{P}_{img} = \mathbf{K} \cdot [\mathbf{R}|\mathbf{t}] \cdot \mathbf{P}_{world}, \quad (1)$$

where  $\mathbf{K}$  is the camera intrinsic matrix with the internal characteristics of the camera, and  $[\mathbf{R}|\mathbf{t}]$  is the camera extrinsic matrix describing how the camera is positioned in the 3D space through rotations and translations. For more details about these components and pin-hole camera model, see [5]. Both matrices need to be correctly calculated in the intrinsic and extrinsic calibration processes, respectively. In the case of the intrinsic parameter calibration, all elements of  $\mathbf{K}$  need to be precisely calculated following the form:

$$\mathbf{K} = \begin{bmatrix} f_x & 0 & c_x \\ 0 & f_y & c_y \\ 0 & 0 & 1 \end{bmatrix} \quad (2)$$

where  $f_x, f_y$  are focal lengths of the camera and  $(c_x, c_y)$  is the principal point, i.e., a point where the optical axis intersects the image. The focal lengths [px] can be derived from the focal length  $f$  [mm] of the camera, assuming we know the pixel width  $s_x$  and height  $s_y$  [mm] as  $f_x = f/s_x$  and  $f_y = f/s_y$ . The principal point is usually in the image center.

In practice, the presented model does not accurately project points on the image plane due to a non-linear disturbing factor such as lens distortion, this leads to a pincushion or barrel effect.

Typically, lens distortion is associated with two components: radial and tangential distortion. The first one affects the distance of the pixels from the center of the image and the second one describes the misalignment of the optical axis with respect to the image center.

Many mathematical models were proposed to describe the physical process of distortion. For fisheye lenses, the Kannala-Brandt model is considered a good option [6]. For other types of lenses, the Brown-Conrady is commonly used [7]. The Brown-Conrady model addresses both radial and tangential distortion that are typically represented by five distortion coefficients:

$$\mathbf{D} = (k_1, k_2, p_1, p_2, k_3). \quad (3)$$

where  $k_1, k_2, k_3$  are radial distortion coefficients and  $p_1, p_2$  are tangential distortion coefficients. To compute the undistorted pixel coordinates according to Brown-Conrady model, we use the following formulas:

$$x_{undistorted} = x_{distorted} + (x_{distorted} - c_x) \cdot (k_1 r^2 + k_2 r^4 + k_3 r^6) \quad (4)$$

$$y_{undistorted} = y_{distorted} + (y_{distorted} - c_y) \cdot (k_1 r^2 + k_2 r^4 + k_3 r^6) \quad (5)$$

where  $r$  is the distance from the principal to the distorted pixel:

$$r = \sqrt{(x_{distorted} - c_x)^2 + (y_{distorted} - c_y)^2}. \quad (6)$$

To find the distortion coefficients, one needs to use a calibration procedure. Zhang proposed a novel calibration technique [8] that could be used in an arbitrary setting. His method for camera calibration uses multiple images of a checkerboard pattern taken from different orientations to estimate the camera's intrinsic parameters.

There are also alternatives to Zhang's method, such as an algorithm using circles instead of checkerboards introduced by Heikkila [9], or an algorithm developed by Rahman and Krouglicof [10], or a numerical calibration algorithm developed by Alvarez et al. [11]. Recently, even deep learning methods have been considered e.g., by Janos and Benesova [12]. These algorithms might come in variations, e.g., the method presented by Chuang and Chen [13] supposedly improving Zhang's algorithm by using checkerboards and principal lines. Duda and Frese proposed a modified checkerboard corner detection for Zhang's method [14].

The lens distortion can influence the correct distance or depth estimation of an object in stereovision systems [3,4]. The standard formula for distance  $d$  between the camera image plane and the scene plane can be calculated with the aid of horizontal  $\Delta x$  or vertical  $\Delta y$  disparity, but we use the latter:

$$d = \frac{f \cdot B}{\Delta y \cdot s_y}, \quad (7)$$

where  $B$  is the baseline and  $s_y$  is the height of a pixel.

### 3. Problem Statement

Although there are a variety of calibration techniques, no statistical analysis of lens distortion effects across a set of cameras of the same type is known. Neither has there been any study on the effect of differences in lens distortion in long-range object-tracking applications. This study aims to fill this gap by applying it to monitoring systems using 3D localisation as a case study.

In this research, we focus on examining the effects of lens distortion among different cameras on the 3D-localisation estimation of the bird approaching wind farms. The following research questions and hypotheses are considered.

**Research Question 1:** What are the effects of lens distortion on stereovision-based distance measurement, and how can they be eliminated?

**Hypothesis 1:** There are two main effects of lens distortion on stereovision-based distance measurement. The first one is caused by the distortion of each camera, which deforms the pictures in different areas of the image at different levels. The second one is caused by differences in lens distortions of various lenses. The common calibration method uses the Zhang-Duda-Frese correction method [8,14] applied to each camera.

**Research Question 2:** How can a lens be classified as an outlier based on distortion level?

**Hypothesis 2:** As a first classification criterion, we propose to classify lenses based on coefficients  $k_1$ ,  $k_2$  and  $k_3$ , and how they deviate from a lens set's average value. As a second classification criterion, we propose to apply a novel measure of linear curvature reduction after the undistortion process compared to the original image.

**Research Question 3:** How to measure the effect of lens distortion of a camera and the consequence of the difference in lens distortions in a stereovision camera pair on distance estimation?

**Hypothesis 3:** To assess the impact of lens distortion, we simulate an ideal straight-line synthetic track of an object moving across the entire field of view of a stereovision

camera pair. After applying the Zhang-Duda-Frese calibration method and the Nelder-Mead optimization technique, the synthetic trajectories are distorted to reflect the effects of lens distortion. The constant disparity and distance for an ideal synthetic trajectory can be compared with the distance and disparity for distorted tracks to quantify the disparity and distance estimation errors. This approach allows us to evaluate the potential improvement achieved through the reverse process, which is distortion correction. The method can be applied to a stereo-camera pair where both lenses have the same or different distortions. In the latter case, the impact of the lens distortion difference on distance estimation error can also be evaluated.

#### 4. Implementation of Lens Distortion Correction

Some distortion correction methods are described in Section 2. In our study, we apply an experiment-based methodology Zhang-Duda-Frese which is popular and easy to use due to its implementation in OpenCV library [15]. In this section, we describe the calibration process and its outcomes.

##### 4.1. Experimental Setup

The research is conducted using a batch of eleven cameras assembled using Raspberry Pi High Quality Camera with a Sony IMX477 matrix [16] and a Basler Lens C125-0618-5m-P with a focal length  $f = 6.0 \pm 0.6$  mm and aperture range F1.8 [17].

For calibration, a checkerboard of  $10 \times 15$  black and white squares is used. The board is printed on an A1 paper sheet 594 mm  $\times$  841 mm and mounted in a frame for stabilisation. The side length of a single square is 52 mm. For evaluation purposes, two additional A1 posters are printed, one with vertical lines connecting shorter sides of the poster, and the other one with horizontal lines connecting longer sides of the poster. Horizontal lines have 55 cm lengths, while the vertical lines have 81.3 cm lengths. All of the lines have 2 mm width and 17 mm gap between each other. Each measure has up to 1 mm measurement error due to measurement technique and used tools.

The calibration environment is a room with strong artificial light and weaker natural light blocked by window blinds. The cameras are installed on a stable mono-pod rig 120 cm above the ground and sharpened using the posters placed at a distance of 2 m. The camera sharpening is evaluated by the staff each time and if the vision is blurry, the process is repeated.

##### 4.2. Calibration Process

All of the calibration images are taken at a distance of 2 m away from the camera. The camera is placed on the stable non-moving rig; one person holds the checkerboard in a desired location while another person evaluates the position, corrects it if necessary, and takes photographs. For every camera, a total of 30 photographs of the checkerboard are taken. This number is experimentally proved to be sufficient to estimate good calibration parameters, even if slight alterations in the checkerboard localization in 3D space or other disturbing factors are considered.

The first nine images are taken with the checkerboard held parallel to the camera scene in different locations (left-middle-right and top-middle-bottom) such that the nine checkerboards covered most of the field of view. The middle top location of the checkerboard can be seen in Figure 1a. Following that, the rest of the images are taken in various field of view locations with a modified checkerboard yaw, see Figure 1b, or modified pitch, see Figure 1c, or slightly altered roll.

Once all the pictures are taken for each camera, the Zhang-Duda-Frese algorithm [8,14] calculates the distortion coefficients of the lens. The matrix  $\mathbf{K}$  is fixed for all cameras with the principal point in the image center as:

$$\mathbf{K} = \begin{bmatrix} 3056 & 0 & 1200 \\ 0 & 3054 & 1600 \\ 0 & 0 & 1 \end{bmatrix} \quad (8)$$



and the radial distortion coefficients  $k_1, k_2$  and  $k_3$  are calculated for each camera using the fixed  $\mathbf{K}$ . Using the distortion coefficients, the calibration process can be applied to an image. Each pixel of the distorted image is moved by a 2D vector defined by formulas (4) and (5). The result of movement is a new corrected image.

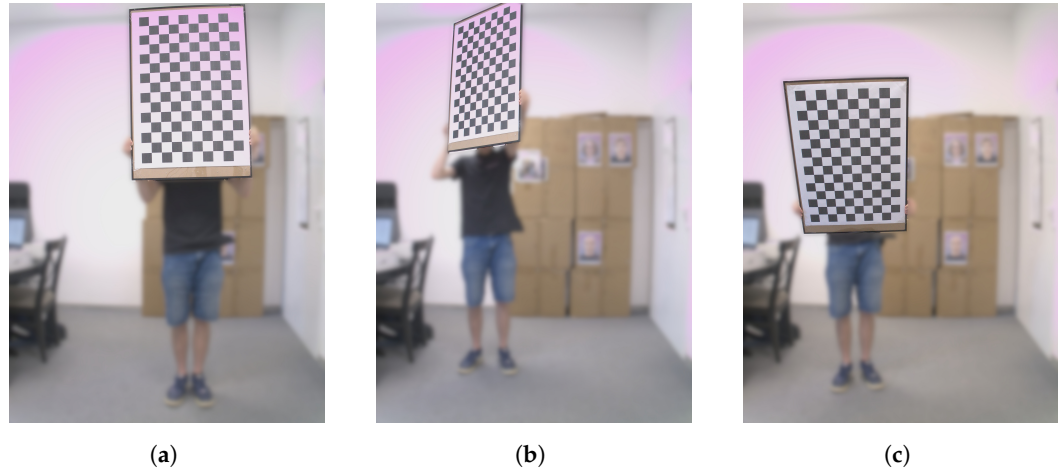


**Figure 1.** Photographs used to calibrate the camera 1751 with blurred background for anonymity. (a) Image with a checkerboard parallel to the camera scene. (b) Image with a checkerboard yaw transformation. (c) Image with a checkerboard pitch transformation.

Examples of the correction process are presented in Figure 2. The estimated distortion coefficients are used to correct the pictures of vertical and horizontal lines taken from a distance of 0.5 m, covering the entire camera view. Figure 2a,c show the images with original lines, while Figure 2b,d show the images after corrections, where blackened parts are the measure of deformation.

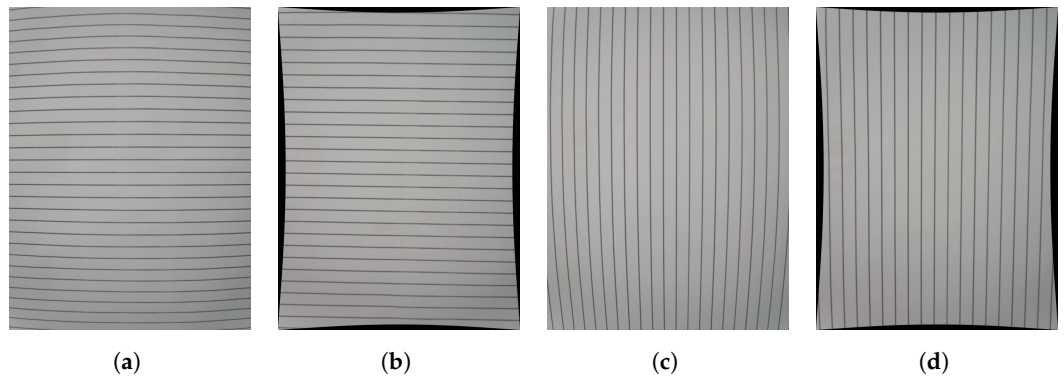


**Figure 2.** Process of lens distortion correction/undistorting. The original images are stretched, especially at the corners. This affects the empty blackened areas in the corrected images. (a) Horizontal lines—original image. (b) Horizontal lines—corrected image. (c) Vertical lines—original image. (d) Vertical lines—corrected image.

#### 4.3. Camera Evaluation Based on Distortion Coefficients

Estimation of distortion coefficients for a set of cameras of the same type can be used to evaluate them, find cameras that can be used for stereovision, and disqualify cameras where outlying distortion coefficients can create big uncertainty in distance measurement. We assume that the cameras whose distortion coefficients vary more than  $2\sigma$  from average values should not be used.

In our experiment, the process for finding distortion coefficients  $k_1, k_2, k_3$  was done for eleven cameras numbered #159, #183, #218, #223, #226, #247, #304, #401, #1726, #1855, and #2182. The calculation results are presented in Table 1. The cells of the table are coloured

to find outlying values, and it can be seen that the distortion coefficients of the camera #1726 deviate most, and therefore the camera should be eliminated from further experiments.

**Table 1.** Distortion coefficients, mean and standard deviation values. For each coefficient, values are tested using  $z.score = (x - mean)/sd$  to find outliers. A value with  $z.score \in [-1, 1]$  is marked with green, for  $z.score \in [-2, -1) \cup (1, 2]$  the value is yellow, for  $z.score \in [-3, -2) \cup (2, 3]$  the value is orange.

		Distortion Coefficients		
		k1	k2	k3
Camera ID	159	-0.217	-0.024	0.158
	183	-0.243	0.067	0.077
	218	-0.235	0.010	0.141
	223	-0.224	0.042	0.053
	226	-0.237	0.027	0.134
	247	-0.241	0.009	0.162
	304	-0.284	0.269	-0.300
	401	-0.266	0.203	-0.192
	1726	-0.200	-0.292	0.828
	1855	-0.262	0.149	-0.112
	2186	-0.247	0.109	-0.041
mean		-0.241	0.052	0.083
sd		0.024	0.145	0.291

To visualise the effect of lens distortion on pixel displacement, heatmaps for cameras #159 and #183 are presented in Figure 3. The difference in pixel displacement between the two cameras is presented in Figure 3c and can reach around 5 px.

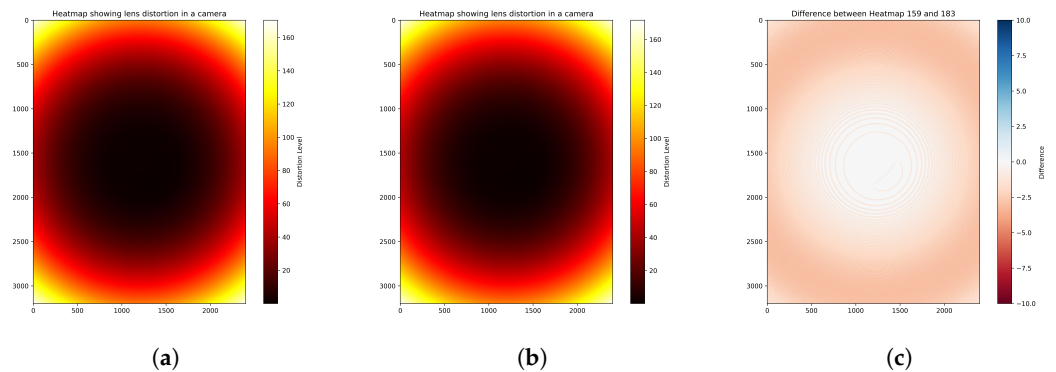


**Figure 3.** Comparison of heatmaps of pixel displacement for camera calibrations. The distortion level is the vector length by which the original pixel should be moved to obtain an undistorted image. (a) Heatmap for calibration of camera 159. (b) Heatmap for calibration of camera 183. (c) Heatmap of differences between heatmap (a) and (b).

### 5. Evaluation of Lens Distortion Correction and Its Impact on Stereovision-Based Distance Measurement

We propose two methods to evaluate the performance of the image corrections. The first one applies the linear regression to measure line curvature before and after correcting distortion. The second one uses the perfect synthetic tracks, distorts them, and calculates the errors in distance estimation.

#### 5.1. Evaluation of Line Curvature Improvement after Lens Distortion Correction

The evaluation method finds how straight vertical and horizontal lines of the template, which are distorted in the original image, are straightened by the distortion correction

method. Firstly, a few pre-processing steps are undertaken. A square kernel filters the pictures to convert them image into black and white. The kernel is an experimentally found square matrix where each row is [8, 8, 4, -4, -12, -12, -12, -4, 4, 8, 8]. Only coherent lines are further processed. For process simplification, the vertical line image is rotated by 90 degrees so that both images have a horizontal orientation.

A novel measure of the curvature of the lines before and after correction is used to assess the correction results. The curvature is measured by the MSE value of differences between the ideal line created by linear regression and the lines from distorted and corrected images, see Figure 4.

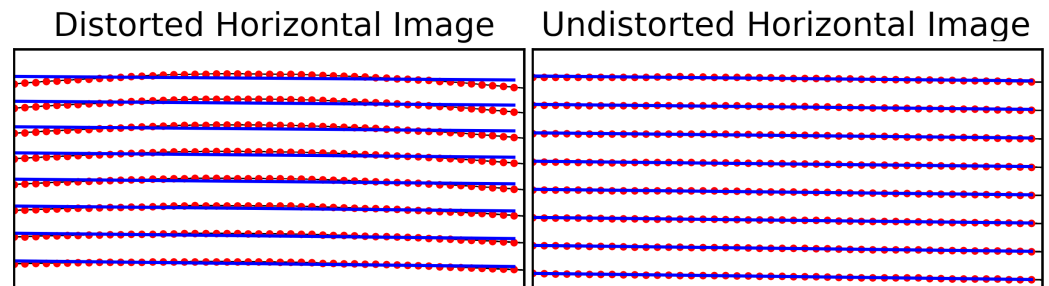


**Figure 4.** The upper part of horizontal line images for camera 183, distorted on the left and corrected on the right. Linear regression is applied to photographed lines in black by taking a sample of points in red. The regression result lines are in blue.

Since some cameras have more lines or regression points than others, an additional normalisation is applied. Due to differences in distortions on the image margins, images are cropped on the sides to ensure that evaluation is done on the same image area. After that, 800 points most distant from the centre of the image are selected. Using these points, we measure their distances from the regression lines and compute mean squared error, MSE, which is used as the evaluation score.

The evaluation results of eight cameras are presented in Table 2 and Table 3 for distorted and undistorted lines, respectively. The MSE values of the distorted images vary from 182 px to 249 px for vertical lines and from 72 px to 117 px for horizontal lines. The MSE values for corrected images vary from 1.9 px to 4.4 px for vertical lines and from 2.3 px to 6.9 px for horizontal lines. From Table 3, it can be concluded that the improvement rate, which is a ratio of MSE before and after calibration, in vertical lines is much bigger than in horizontal ones, 81.4 vs. 28.3. The mean improvement of specific cameras varies from 30.8 for camera 218 to 75.4 for camera 218. Such big differences in improvement prove the effectiveness of the correction method.

**Table 2.** Linear regression evaluation results for distorted lines. MSE is calculated using two photos from each camera.

	Camera ID							Mean [px]
	159	183	218	223	226	401	2186	
Vertical [px]	185.4	182.0	249.1	224.6	217.4	210.4	212.9	211.7
Horizontal [px]	114.4	116.6	71.6	99.5	107.1	117.3	106.5	118.9
Mean [px]	149.9	149.3	160.3	162.1	162.2	163.8	165.9	159.1

**Table 3.** Linear regression evaluation results for corrected lines (after calibration). MSE is calculated using two photos from each camera.

	Camera ID							Mean	Improvement
	159	183	218	223	226	401	2186	[px]	Rate
Vertical [px]	1.9	1.8	3.5	4.4	2.7	2.2	2.0	2.6	81.4
Horizontal [px]	4.4	2.5	6.9	5.0	3.7	4.8	2.3	4.2	28.3
Mean [px]	3.1	2.1	5.2	4.6	3.2	3.5	2.2	3.4	46.8
Improvement Rate	48.4	71.1	30.8	35.2	50.7	46.8	75.4	46.8	

Cameras 247 and 1855 have been excluded from the set of test cameras because of their outlying MSE values for corrected images, 13.02 px and 20.12 px, respectively.

### 5.2. Evaluation of Lens Distortion Effect on Stereovision

This research also involves testing how the lens distortion affects an object's distance estimation at long-range using stereo-cameras. The proposed method uses data from camera tests and synthetically generated long-range flight paths. Cameras' technical specifications are mentioned in Section 4.1 and distortion coefficients are given in Table 1. The experiment use a BPS layout with cameras mounted vertically with a baseline of  $B = 1$  m [4]. The estimation of distance  $d$  [m] is calculated based on (7) with the height of each pixel  $s_y = 0.006287$  mm according to the camera's technical specification [16,17].

The following experiments must ensure that undistorted and distorted images have the same size, 2400 px  $\times$  3200 px. We simulate a bird's flight at constant distances defined by the disparity between two lines. Assuming both stereo-cameras have no lens distortion, the lines would map the bird's trajectory as two parallel horizontal lines. The line on the bottom camera is  $\Delta y$  pixels above the top one. Both lines are placed in the uppermost part of the camera images, where they are strongest affected by lens distortion, see Figure 3.

In this section, the following notation is used: the *top camera* is the camera placed above the *bottom camera*, and in the coordinate system with a reference point in the matrix middle, it sees the objects, which are above its optical axis closer to the matrix middle than the *bottom camera*. However, in image processing, the coordinates are usually related to the left top corner of the images, so the *top line* corresponds to the bottom camera, and vice versa, the *bottom line* corresponds to the top camera.

The two parallel lines are a series of points in each camera's frame with a constant value of  $y$ , and  $x$  varying from 0 to 2400. Then each line is distorted using the algorithm, which applies distortion coefficients for a process of reverting correction. It is done using a numerical algorithm implementing Nelder-Mead optimization method. The algorithm iteratively searches for the distorted pixel coordinates given an undistorted pixel. This method ensures precision in five decimal places. The methodology is applied to two settings of lines:

- **Track 1:**  $y_{top} = 95$  px,  $y_{bottom} = 100$  px,  $\Delta y = 5$  px corresponding to  $d = 600$  m
- **Track 2:**  $y_{top} = 95$  px,  $y_{bottom} = 105$  px,  $\Delta y = 10$  px corresponding to  $d = 300$  m.

The experiments with the synthetic track evaluation method use distortion coefficients of cameras 159, 183, and 2186. A visualisation of the method is presented in Figure 5, which illustrates four cases. Figure 5a and Figure 5b show Track 1 and Track 2 respectively for camera 159. Figure 5c and Figure 5d show Track 1 for a pair of cameras 183 and 2186 in the reverse constellation. Note that reversing the order of the cameras, top with bottom, strongly affects the disparity between cameras, see Figure 5c,d.

To evaluate how differences in distortions of different lenses could affect the non-corrected measurement, we test a case when the same camera is used in a stereovision set. For each track and each camera pair, a few measures are calculated: minimal and maximal distorted track disparity [px], and their corresponding distances [m] estimated using (7) and their deviation from the original, corrected values in [%]. The results are shown in Table 4.

Table 4 shows the experimental results for the nine combinations of three cameras for each of two Tracks. The stereo cameras with the same distortion coefficients are along the table diagonal. The results are consistent since the errors in disparities and distances for both tracks' range from +17% to +20%. This ideal case would be where all the lenses and cameras are consistently manufactured and assembled.

In reality, a stereovision pair consists of two cameras with different distortion coefficients, which is illustrated in non-diagonal cells of Table 4. Lenses with different distortions for top and bottom cameras cause bigger errors. In some cases, the distance becomes shorter, e.g., for a pair with top camera 159 and bottom camera 2186, with an distance error between 34% and 41%. In the case of top camera 183 and bottom camera 159 for **Track 1**, the distance appears much larger, between 96% and 302%. Sometimes, the disparity falls to 0 px or a negative value, giving a false infinity position.

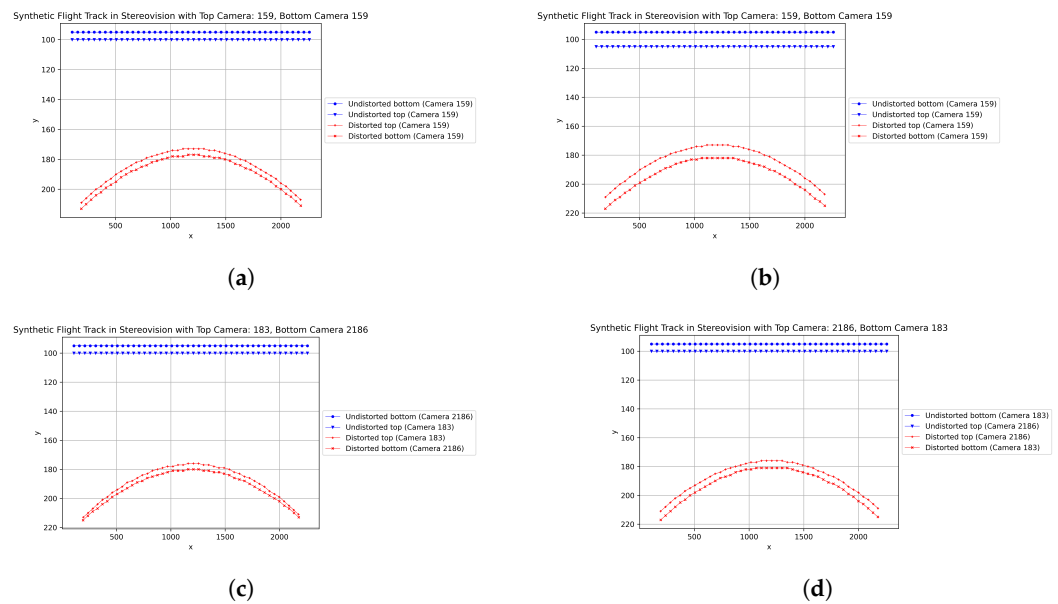


**Figure 5.** Comparison of synthetic bird tracks before (blue) and after (red line) distortion. (a) Undistorted and distorted **Track 1** for camera 159. (b) Undistorted and distorted **Track 2** for camera 159. (c) Undistorted and distorted **Track 1** for top camera 183 and bottom camera 2186. (d) Undistorted and distorted **Track 1** for top camera 2186 and bottom camera 183.

**Table 4.** Impact of lens distortion on stereovision measured for camera pairs using the synthetic bird tracks. Table cell colours emphasise errors going up to 20% (green), then up to 100% (yellow) and above 100% (red).

Max and min errors in disparity and distance for distorted <b>Track 1</b> ( $\Delta y = 5$ px, $d = 600$ m)			
Top $\downarrow$ , Bottom $\rightarrow$	159	183	2186
159	-0.7 px $\rightarrow$ 105 m (+17%) -0.8 px $\rightarrow$ 112 m (+19%)	2.3 px $\rightarrow$ -187 m (-32%) 0.9 px $\rightarrow$ -90 m (-15%)	3.5 px $\rightarrow$ -246 m (-41%) 2.5 px $\rightarrow$ -202 m (-34%)
183	-2.4 px $\rightarrow$ 576 m (+96%) -3.8 px $\rightarrow$ 1814 m (+302%)	-0.7 px $\rightarrow$ 105 m (+17%) -0.8 px $\rightarrow$ 110 m (+18%)	1.8 px $\rightarrow$ -169 m (-27%) -0.5 px $\rightarrow$ 162 m (+10%)
2186	-3.0 px $\rightarrow$ 2540 m (+423%) -5.0 px $\rightarrow$ $+\infty$ m	-1.0 px $\rightarrow$ 156 m (+26%) -3.4 px $\rightarrow$ 1302 m (+217%)	-0.8 px $\rightarrow$ 107 m (+18%) -0.8 px $\rightarrow$ 107 m (+18%)
Max and min errors in disparity and distance for distorted <b>Track 2</b> ( $\Delta y = 10$ px, $d = 300$ m)			
Top $\downarrow$ , Bottom $\rightarrow$	159	183	2186
159	-1.5 px $\rightarrow$ 52 m (+17%) -1.6 px $\rightarrow$ 56 m (+19%)	1.5 px $\rightarrow$ -40 m (-13%) 0.1 px $\rightarrow$ -3 m (-1%)	2.6 px $\rightarrow$ -63 m (-21%) 1.8 px $\rightarrow$ -45 m (-15%)
183	-3.2 px $\rightarrow$ 143 m (+48%) -4.5 px $\rightarrow$ 245 m (+82%)	-1.5 px $\rightarrow$ 52 m (+17%) -1.5 px $\rightarrow$ 52 m (+17%)	1.0 px $\rightarrow$ -27 m (-9%) -1.2 px $\rightarrow$ 42 m (+14%)
2186	-4.8 px $\rightarrow$ 275 m (+92%) -5.9 px $\rightarrow$ 429 m (+143%)	-1.8 px $\rightarrow$ 65 m (+22%) -4.2 px $\rightarrow$ 217 m (+72%)	-1.5 px $\rightarrow$ 53 m (+18%) -1.7 px $\rightarrow$ 60 m (+20%)

The presented results show that removing lens distortion is crucial for accurate object localisation, especially in the affected image parts, i.e., the corners and margins. Correction is essential in monitoring a long-range stereovision system, such as BPS. The system has to make autonomous decisions when a large bird of prey approaches a wind turbine at a 400 m distance to be able to stop the rotor in time. As shown, distances of 600 m and 300 m could be falsely estimated and appear as long and safe, while it could be too late to undertake a necessary reaction.

## 6. Results and Conclusions

The calibration process of each camera uses a checkerboard with non-standardized positioning and consists of a significant number of calibration images. The process relies on a large number of images and their stable positioning rather than positional precision. Calibration parameters are unique to a given camera. The differences in the distribution of distortion coefficients can cause calibration problems. Therefore, the cameras, which vary more than  $2\sigma$  from the set of cameras, should not be used especially for stereovision applications.

The evaluation method of the correction quality can be based on linear regression lines. A statistical comparison of results can help to eliminate cameras that deviate from the average measurements. The  $2\sigma$  criterion seems to be suitable for camera selection.

Using synthetic tracks simulating bird flights is a way to check and evaluate the effect of lens distortion on stereovision applications. The presented results show that the effect can be considered as a linear systematic error of value less than 20% but only in the case when both cameras have the same parameters. For cameras with different lens parameters, the error can be big up to 400% or even be considered a mistake due to the impossible relationship between object localisation on the top and bottom camera. However, the calibration of lens distortion can correct the error. Nevertheless, careful consideration of paring cameras would be recommended.

The methods and results presented in this paper are preliminary steps for future research. The next step would focus on improving the distortion correction algorithm or model, which can be based on the Machine Learning approach. Apart from this, a synthetic 3D bird's flight trajectory could evaluate the tracking error of the movement in different areas of lenses. Also, a statistical analysis of lens parameter distributions for a large number of cameras is an interesting issue.

**Author Contributions:** Conceptualization, D.G., W.J.K., W.K.; methodology, G.M., W.K., W.J.K.; software, G.M., S.Z., M.K.; validation, G.M.; formal analysis, G.M., W.J.K.; investigation, G.M.; resources, D.G.; data curation, S.Z., M.K.; writing—original draft preparation, G.M.; writing—review and editing, W.J.K.; visualization, G.M., S.Z., M.K.; supervision, W.J.K.; project administration, D.G.; funding acquisition, D.G., W.J.K. All authors have read and agreed to the published version of the manuscript.

**Funding:** This research was funded by The National Centre for Research and Development of Poland grant number POIR.01.02.00-00-0247/17. Project title: 'Realization of R&D works leading to the implementation of a new solution - MULTIREJESTRATOR PLUS for monitoring and control of the power system in terms of operational efficiency, the life span extending and optimizing the impact on the surrounding wind farms'.

**Institutional Review Board Statement:**

**Informed Consent Statement:**

**Data Availability Statement:** The data presented in this study are available on request from the corresponding author.

**Conflicts of Interest:** The authors declare no conflicts of interest. The funders had no role in the design of the study; in the collection, analyses, or interpretation of data; in the writing of the manuscript; or in the decision to publish the results.



## References

1. van Erp, T.; Carvalho, N.G.P.; Gerolamo, M.C.; Gonçalves, R.; Rytter, N.G.M.; Gladysz, B. Industry 5.0: A new strategy framework for sustainability management and beyond. *J. Clean. Prod.* **2024**, *461*, 142271. <https://doi.org/10.1016/j.jclepro.2024.142271>.
2. Gradolewski, D. Sensors and Algorithms in Industry 4.0: Security and Health Preservation Applications. Ph.D. Thesis, Blekinge Tekniska Högskola, Karlskrona, Sweden, 2021.
3. Gradolewski, D.; Dziak, D.; Kaniecki, D.; Jaworski, A.; Skakuj, M.; Kulesza, W.J. A Runway Safety System Based on Vertically Oriented Stereovision. *Sensors* **2021**, *21*, 1464. <https://doi.org/10.3390/s21041464>.
4. Gradolewski, D.; Dziak, D.; Martynow, M.; Kaniecki, D.; Szurlej-Kielanska, A.; Jaworski, A.; Kulesza, W.J. Comprehensive Bird Preservation at Wind Farms. *Sensors* **2021**, *21*, 267. <https://doi.org/10.3390/s21010267>.
5. Hartley, R.; Zisserman, A. *Multiple View Geometry in Computer Vision*; Cambridge University Press: Cambridge, UK, 2003.
6. Kannala, J.; Brandt, S.S. A generic camera model and calibration method for conventional, wide-angle, and fish-eye lenses. *IEEE Trans. Pattern Anal. Mach. Intell.* **2006**, *28*, 1335–1340.
7. Brown, D. Decentering distortion of lenses. *Photogramm. Eng.* **1966**, *32*, 444–462.
8. Zhang, Z. A flexible new technique for camera calibration. *IEEE Trans. Pattern Anal. Mach. Intell.* **2000**, *22*, 1330–1334. <https://doi.org/10.1109/34.888718>.
9. Heikkila, J. Geometric camera calibration using circular control points. *IEEE Trans. Pattern Anal. Mach. Intell.* **2000**, *22*, 1066–1077. <https://doi.org/10.1109/34.879788>.
10. Rahman, T.; Krouglicof, N. An Efficient Camera Calibration Technique Offering Robustness and Accuracy Over a Wide Range of Lens Distortion. *IEEE Trans. Image Process.* **2012**, *21*, 626–637. <https://doi.org/10.1109/TIP.2011.2164421>.
11. Álvarez, L.; Gómez, L.; Sendra, J.R. An Algebraic Approach to Lens Distortion by Line Rectification. *J. Math. Imaging Vis.* **2009**, *35*, 36–50. <https://doi.org/10.1007/S10851-009-0153-2>.
12. Janos, I.; Benesova, W. Improving radial lens distortion correction with multi-task learning. *Pattern Recognit. Lett.* **2024**, *183*, 147–154. <https://doi.org/https://doi.org/10.1016/j.patrec.2024.05.008>.
13. Chuang, J.H.; Chen, H.Y. Alleviating Radial Distortion Effect for Accurate, Iterative Camera Calibration Using Principal Lines. *IEEE Trans. Instrum. Meas.* **2024**, *73*, 1–11. <https://doi.org/10.1109/TIM.2024.3436097>.
14. Duda, A.; Frese, U. Accurate Detection and Localization of Checkerboard Corners for Calibration. In Proceedings of the British Machine Vision Conference, Newcastle, UK, 3–6 September 2018.
15. Bradski, G. The OpenCV Library. *Dr. Dobb's J. Softw. Tools* **2000**, *120*, 122–125.
16. Raspberry Pi High Quality Camera. Available online: <https://datasheets.raspberrypi.com/hq-camera/hq-camera-product-brief.pdf> (accessed on 14 October 2024).
17. Sony IMX477 Matrix. Available online: <https://docs.baslerweb.com/c125-0618-5m-p> (accessed on 14 October 2024).

**Disclaimer/Publisher's Note:** The statements, opinions and data contained in all publications are solely those of the individual author(s) and contributor(s) and not of MDPI and/or the editor(s). MDPI and/or the editor(s) disclaim responsibility for any injury to people or property resulting from any ideas, methods, instructions or products referred to in the content.